Quantifying implications of deposit aging from crude refinery preheat train data

Edward Masato Ishiyama[a], Erik Falkeman[b], David Ian Wilson[c] and Simon John Pugh[a]

[a] Heat Transfer Research, Inc., Navasota, Texas, USA

[b] Preem Raffinaderi AB, Göteborg, Sweden

[c] Department of Chemical Engineering and Biotechnology, University of Cambridge, Philippa Fawcett Drive, Cambridge, CB3 0AS, UK

Address correspondence to Dr Edward Ishiyama, Heat Transfer Research, Inc., P.O. Box 1390, Navasota, TX 77868 USA. E-mail: edward.ishiyama@htri.net Phone Number: (+1) 979 690 5050, Fax Number: (+1) 979 690 3250

ABSTRACT

Heat exchanger fouling has been studied for some time in the petroleum industry. As understanding of fouling dynamics and mitigation methods improves, refinery fouling mitigation strategies are changing. The implications of deposit aging in refinery units have not been addressed in detail: aging refers to where the deposit undergoes physical and chemical conversion over time. In the 2009 Heat Exchanger Fouling and Cleaning conference, Wilson et al. [Ageing: Looking back and looking forward] presented a simple framework illustrating how deposit aging impacts heat exchanger thermal and hydraulic performance. This paper presents insights into deposit aging gained from analysis of refinery monitoring data. Two case studies are presented: (i) one from the Preem refinery in Sweden where stream temperature, flow and gauge pressure measurements indicated a higher deposit thermal conductivity in exchangers located in the hotter section of the preheat train. (ii) US refinery stream temperature, flow and plant cleaning log data, showing an increased resistance to cleaning when deposits are exposed to high temperature for a prolonged period. The use of deposit aging analysis to improve exchanger operation is discussed.

INTRODUCTION

Fouling is a persistent problem in petroleum refinery heat exchangers and continues to be studied by both academia and industry. As a result, the impact of fouling in refinery exchangers is changing due to better selection of crudes, innovative heat exchanger and network design, rigorous performance monitoring and process optimization. Aging is another aspect of fouled deposits that have an important role in dictating the thermo-hydraulic performance of heat exchangers as well as cleaning of the units. Aging in this manuscript is the process whereby fouling deposits undergo chemical and physical changes over time. The process is accelerated and enhanced when the deposit is in contact with a heated surface.

Epstein [1] identified aging as one of the principal mechanistic steps in fouling. A brief review of subsequent work in deposit aging was presented in the 2009 Heat Exchanger Fouling and Cleaning conference alongside a simple, first order kinetic model of aging in chemical reaction fouling, linking heat transfer and the evolution of deposit thermal conductivity [2,3].

This model was implemented by Coletti et al. [4] within a dynamic, distributed simulation of crude oil fouling in a shell and tube heat exchanger, incorporating spatial and temporal distributions. Subsequent work by Ishiyama et al. [5] revisited the modeling of aging deposits where chemical reaction was the major mechanism for deposition. A simpler, two-layer, concept to represent deposit aging was introduced, similar to that proposed by Atkins [6]. This has computational merit, being simple to incorporate into heat exchanger and plant simulations. Ishiyama et al. [7] demonstrated its use in the identification of cleaning schedules where the effectiveness of the cleaning action depended on the cleaning method. [7], [8] extended the approach to biofouling where cleaning actions can also determine

whether an induction period is observed after the unit is brought back on-line. This concept is revisited here via its application to a refinery heat exchanger.

Table 1 [9] summarizes deposit thermal conductivity values reported in the literature. These are compared with estimates obtained by analyzing plant monitoring data from crude refinery heat exchangers. This information represents one of the first studies of deposit aging in industrial units and the implications for operating and cleaning are discussed.

METHODOLOGY

The objective of the analysis is to use available plant monitoring data to estimate the thermal conductivity of fouling deposits generated from the crude stream. To simplify the presentation, exchangers with crude on the shell side and exchangers with fouling contributions from the product stream are not discussed here. For exchangers the temperatures, flow rates and gauge pressures were monitored and recorded, where available. The tubeside crude gauge pressure measurements were used to monitor crude-side pressure drop and estimated the change in fouling layer thickness. The following steps were followed in the analysis.

Step 1: Monitor the stream flow rates, inlet and outlet temperatures, and tubeside pressure drop on the exchanger.

Step 2: Simultaneously calculate the overall fouling resistance, R_f, and the tubeside deposit thickness, δ, based on the thermal and hydraulic performance of the unit.

Step 3: For exchangers with crude on the tube side and no shellside fouling, calculate the average deposit thermal conductivity λ_f using the thin slab relationship given by

$$\lambda_f = \frac{\delta}{R_f} \tag{1}$$

Heat transfer

The overall heat transfer coefficient, *U*, of an exchanger is evaluated based on the sum of resistances in series:

$$\frac{1}{U} = \frac{1}{h_o} + R_{f,o} + \frac{d_o \ln\left(\frac{d_o}{d_i}\right)}{2\lambda_w} + \frac{d_o}{d_i} R_{f,i} + \frac{d_o}{d_i}\frac{1}{h_i} \tag{2}$$

Here h_i is the internal heat transfer coefficient, h_o the external heat transfer coefficient, $R_{f,o}$ the external fouling resistance, $R_{f,i}$ the internal fouling resistance, δ the deposit thickness and d_i and d_o are the internal and external tube diameters, respectively. $R_{f,o}$ is taken to be zero for exchangers with product on the shell side and in the absence of product stream fouling, making $R_{f,i}$ equal to the overall thermal resistance of the deposit, R_f.

h_i is a function of the tube-side Fanning friction factor, C_f, which is in turn dependent upon surface roughness, ε, and the flow velocity (Reynolds number, *Re*), as described by the Colebrook-White equation. An explicit form is presented by Sousa et al. [10]:

$$\frac{1}{\sqrt{C_f}} = -4\left(log_{10}\left|\frac{\varepsilon}{3.7\left(d_i - 2\delta\right)}\right| - \frac{5.16}{Re} log_{10}\left|\frac{\varepsilon}{3.7\left(d_i - 2\delta\right)} + \frac{5.09}{Re^{0.87}}\right|\right) \tag{3}$$

For turbulent flow, the relationship developed by Gnielinski [11] for h_i can be used.

$$h_i = \left(\frac{\lambda_f}{d_i - 2\delta}\right) \frac{\left(\frac{C_f}{2}\right)(Re - 1000)Pr}{1 + 12.7\left(\frac{C_f}{2}\right)(Pr^{0.67} - 1)} \quad (4)$$

The correlation is valid for $0.5 \leq Pr \leq 2000$ and $3000 \leq Re \leq 5 \times 10^6$. Here, λ_f is the fluid thermal conductivity and Pr is the Prandtl number.

For the calculation of shell-side heat transfer coefficient, h_o, a stream analysis method is used. An open literature method for obtaining h_o is described in ESDU [12].

The thermal performance of the exchanger can also be expressed as a fouling Biot number, Bi_f, given by:

$$Bi_f = U_{cl} R_f \quad (5)$$

where U_{cl} is the overall fouling resistance in the clean condition.

Pressure drop

The tubeside pressure drop is calculated as the sum of the following losses (e.g. Sinnott [13]):

- Nozzle loss
- Tube entrance, expansion and turn-around losses
- Total tube pressure drop

A simplified representation of the pressure drop, ΔP, takes the form (Ishiyama et al. [14]):

$$\Delta P \approx a\, m^2 + b\, m^{1.75}(d_i - 2\delta)^{-4.75} \quad (6)$$

where *m* is the mass flow rate; *a* and *b* are dimensional constants. The calculation is sensitive to the friction factor which is a function of surface roughness, *e*.

Fouling

The rate of fouling deposition is modelled using the following chemical reaction fouling model [15]

$$\frac{d\delta}{dt} = \lambda_g k_g = \lambda_g \frac{\alpha}{h_i} \exp\left(-\frac{E_F}{RT_{film}}\right) f(\tau) \quad (7)$$

Here, $\lambda_g$is the thermal conductivity of fresh deposit, k_g the deposition rate, α the fouling propensity factor, E_F the fouling activation energy (temperature dependency), R the gas constant, T_{film} the film temperature, and τ the wall shear stress. The subscript g refers to fresh deposit (taken to be a form of gel) while and c refers to aged material ('coke'), as presented by Wilson et al. [3]. $f(\tau)$ is given by

$$f(\tau) = 1 - \left(\frac{\tau - 2}{98}\right)^{0.5}, when\ \tau > 2\ Pa$$
$$else\ f(\tau) = 1 \quad (8)$$

Aging

The two-layer model [5] and the distributed model [2] are summarized in this section. Both are referred to in subsequent discussions.

Two-layer model: The deposit is treated as a pair of thin slabs of insulating material, giving

$$R_f = \frac{\delta_{eff}}{\lambda_{eff}} = \frac{\delta_g}{\lambda_g} + \frac{\delta_c}{\lambda_c} \quad (9)$$

Here, δ_{eff} is the combined deposit thickness, and λ_{eff} is the effective deposit thermal conductivity. The change in thickness of each layer with time, *t*, is assumed to follow zero-order kinetics given by:

$$\frac{d\delta_g}{dt} = \lambda_g k_g - \frac{d\delta_c}{dt} \quad (10)$$

$$\frac{d\delta_c}{dt} = \lambda_c k_c, \delta_g > 0 \quad (11)$$

$$\frac{d\delta_c}{dt} = 0, \delta_g = 0 \quad (12)$$

The $\lambda_g k_g$ term describes the deposition of fresh deposit at the crude/deposit interface: k_c and k_g are the coking and deposition rate constants, respectively. Aging related shrinkage or expansion is not considered here.

Distributed model: Deposit aging is modelled as a gradual change in deposit thermal conductivity from an initial 'fresh (gel)' value of λ_g to a final, 'aged (or coked)' value of λ_c, given by the simple relationship:

$$\lambda_f = \lambda_c + (\lambda_g - \lambda_c)y \quad (13)$$

The parameter y is a youth factor that changes from 1 to 0 as the deposit spends longer in contact with a heated surface. Its evolution is described by a first order decay, viz.:

$$\frac{dy}{dt} = -k_a y \qquad (14)$$

The decay constant, k_a, is deemed to depend on the local temperature within the deposit (which changes with time):

$$k_a = A_a \exp(-\frac{E_a}{RT}) \qquad (15)$$

Here E_a is the aging activation energy and A_a a prefactor.

Thermal and hydraulic performance calculations yield values of R_f and δ. Equation (1) gives λ_f, and the minimum and the maximum values of λ_f give insight into the parameters λ_g and λ_c. Parameters α, k_a, and k_c are extracted from the time series data. The parameter, α, in the deposition model (Equation 7) is likely to be directly related to the crude composition, whereas parameters, k_a and k_c in the aging models are likely to be related to the deposit properties and are thus linked to crude composition but not as strongly as α.

CASE STUDIES

CASE STUDY 1: Preem Göteborg Refinery

Preem is Sweden's largest refiner with 80% of Swedish refining capacity. The case study presented here is based on a section of the preheat train of its refinery in Göteborg. In the preheat train section, the crude is pumped from storage tanks through a set of shell-and-tube

heat exchangers which raise its temperature from ambient to about 130 °C before entering the desalter. The desalter washes the crude with water to remove inorganic impurities. The desalted crude is then pumped and split into 5 branches through a set of exchangers which heat it to temperatures ranging from about 250 to 280 °C. The branches merge and ultimately enter a furnace to receive additional heat before crude entering the distillation column. Figure 1 shows the layout of the section of the preheat train downstream of the desalter. Pressure drop measurements were made at the entrance and exit of each group of exchangers. Three examples of exchanger groups that are discussed here are indicated on the figure (E45, E5AB and E50ABC). All these units had crude on the tube side. The shell-side streams were LCR (lower circulating reflux), HLGO (heavy light gasoil) and MCR (middle circulating reflux), which are less prone to fouling during cooling, so it was reasonable to assume that fouling was restricted to the tube side. In addition there was little product-side deposition observed during cleaning of these units.

Table 2 is a summary of the heat transfer area and operating conditions for the selected units. As the surface roughness of the fouling deposits was unknown, the sensitivity of the pressure drop calculated using Equation (6) to this parameter was determined by using two values of the roughness parameter, namely 43 μm and 200 μm, in the friction factor calculation. These values represent bounds on the roughness parameter based on inspect of deposits.

Plant monitoring and data analysis was conducted using the SmartPM software tool.

The crude feedstock processed at the refinery is a combination of different blends processed over different time scales. The crude blends vary as a result of economic factors. In this analysis observations are made for periods where the crude blends remained relatively

similar. The crude blends differed between periods and cannot be presented for reasons of commercial confidentiality.

A range of thermal conductivity values were extracted for E50ABC, E5AB and E45. These are summarized in Figure 2 along with the operating crude-side surface temperatures of the exchangers. The maximum observed thermal conductivity exhibits a trend to increase with the exposed surface temperature. The values all lie in the range presented in Table 1. There is noticeable variability in the distributions.

Analysis of E45 is discussed in detail in the next section.

Analysis of E45

E45 is the unit with the largest heat transfer area in the network. The unit consists of about 1500 tubes per shell and 4 tubeside passes. Monitoring data indicated that the unit operated at a tubeside shear stress greater than 5 Pa. In the following analysis, the uncertainties were accounted through assuming an uncertainty of ± 10 % in the measured pressure drop.

Observation 1 (time period A): An increase in fouling resistance was accompanied by an increase in deposit thickness (Figure 3 (i) and (ii)). The exchanger did not start in the clean condition so there is a noticeable initial extent of fouling (corresponding to $Bi_f \approx 0.5$) The associated deposit thermal conductivity (Figure 3 (iii)) showed a gradual decrease over time. There is a noticeable effect of surface roughness values to illustrate the influence of the roughness to the methodology.

One explanation for the reduction in estimated thermal conductivity is the deposition of fresh foulant (with lower thermal conductivity) on existing, aged deposit (with higher thermal

conductivity), resulting in a lower effective thermal conductivity, λ_{eff}, for the combined deposit thickness δ_{eff} (see Equation (6)).

For this period, the surface temperature in E45 ranged from 220 °C to 240 °C; the surface shear stress ranged from 7 to 15 Pa (Figure 4). Fitting the fouling data to Equation (7) gave a deposition constant, α, of 50 h^{-1} (assuming a E_f of 43.3 kJ mol^{-1} (activation energy for maltene decomposition). h_i and T_{film} varied between 1500 – 2000 W m^{-2} K^{-1} and 200 – 230°C, respectively.

Fitting the two-layer model (Equation (9)) to the data in Figure 3 gave λ_g to lie in the range 0.18 to 0.20 $Wm^{-1}K^{-1}$, assuming a surface roughness of 200 μm, and between 0.19 and 0.22 W m^{-1} K^{-1} for a surface roughness of 43 μm. These ranges are similar to pitch and amorphous asphalt, which is consistent with the assumption of a softer, gel-like deposit.

Observation 2 (time period B): The deposit thickness extracted from pressure drop measurements remained almost constant over this time period. There was, however, a reduction in fouling resistance (Figure 5) accompanied by a gradual increase in λ_{eff}. This could arise because the combination of crude blend and operating conditions here resulted in almost no deposition and aging of the existing material. The λ_{eff} values are larger than those in Figure 3 (iii).

From the two-layer model, differentiation of Equation (9) gives:

$$\frac{dR_f}{dt} = \frac{1}{\lambda_g}\left(\lambda_g k_g - \frac{d\delta_c}{dt}\right) + \frac{1}{\lambda_c}\frac{d\delta_c}{dt} \qquad (16)$$

As there is no deposition in this period, k_g = 0. By substituting Equation (11) into Equation (16) gives the following result for k_c:

$$k_c = \frac{\frac{dR_f}{dt}}{\left(\frac{\lambda_c}{\lambda_g} - 1\right)} \qquad (17)$$

Taking λ_g = 0.1 W $m^{-1}K^{-1}$ and λ_c = 0.9 W m^{-1} K^{-1}, from the gradient of Figure 5(i), k_c is estimated to be in the range of 0.1 - 2 (10^{-3}) m^2 K W^{-1} h^{-1}.

Fitting the data in Figure 5 to the distributed model (equations (13) and (14)), indicated that the deposit present at the beginning of this monitoring period consisted of an aged deposit of age about 20 to 23 days subject to a decay constant, k_a, between 0.04 and 0.07 day^{-1}. The predictions of the distributed model (Equation (13)) are plotted in Figure 5 and show good agreement with the data. This is not surprising, however, as the parameters were obtained by fitting to the data set. Nevertheless, the identification of a period with no layer growth has allowed the impact of aging to be determined directly. If similar behavior was observed at different operating surface temperatures, the aging parameters A_a and E_a could be estimated.

This case study has demonstrated how temperature, flow and pressure drop measurements can be analyzed to extract estimates of deposit thermal conductivity. Hydraulic measurements are essential for this task. The observations of reduction in deposit thermal conductivity accompanied by constant deposit thickness constitute strong evidence that aging does occur in practice. The deposits were not analyzed, so confirmation of aging either requires further testing with shut downs to obtain samples, or laboratory experiments.

CASE STUDY 2: US Refinery

This case study considers the performance of on an individual heat exchanger located downstream of the desalter on a US refinery. Monitoring data were collected over 3 years and data reconciliation was performed to generate the exchanger performance plots in Figure 6. Details of the cleaning events are given in Table 3. There was a plant shutdown at the end of year 2008. Some bypass actions were not recorded and were not taken into account in the calculations.

The R_f–time data show noticeable changes after cleaning events. The fouling resistance following cleaning gradually increases after each gas oil wash (B, C and D), indicating a reduction in cleaning effectiveness. This could be interpreted as due to the build-up of a sublayer which is harder to remove. A gas oil wash tends to be a cheaper and faster option than mechanical cleaning (e.g. hydro blasting) but at the cost of reduced effectiveness of cleaning after repeated cleans [7]. The rate of coke layer formation can be approximated by the dashed line in Figure 6.

The operator (i.e. the refinery) is interested in knowing both *when* to clean the unit and *which* method to use for cleaning (e.g. gas oil wash vs. hydroblasting). Chemical cleaning methods (e.g. gas oil wash in this context) employ less severe mechanical forces alongside cleaning chemistry and are unlikely to remove all the deposit formed by chemical reaction fouling. A combination of chemical cleans will then eventually require a mechanical clean in order to remove aged deposit and restore the unit to its original clean state. The pattern will

then repeat itself, unless the parameters change over time (e.g. due to changes in crude slate or process configuration). The total length of time, from the unit starting in its clean condition to the point when a mechanical cleaning is completed, is defined as the cleaning 'super-cycle' time, t_{cycle} (see Ishiyama et al. [7]).

Identification of the optimal super-cycle requires minimization of the objective function, $\emptyset_{super}$, [7], [8] :

$$\phi_{super} = \frac{1}{t_{super} \equiv \tau_m + j\tau_c + \sum_{i=1}^{j} t_{c,i} + t_m} \times \left\{ jC_c + C_M + \sum_{i=1}^{j} C_E \int_{t_{c,j-1}+\tau_c}^{t_{c,j}} \left(Q_{cl} - Q(t)\right) dt + \sum_{i=1}^{j} C_E \int_{t_{c,j}+\tau_c}^{t_m} \left(Q_{cl} - Q(t)\right) dt + jQ_{cl}\tau_c + Q_{cl}\tau_m \right\} \quad (18)$$

Here t is time, ϕ_{super} is the total average cost, t_k is the time taken for cleaning action k, Q is the heat duty, C_c is the cost of a chemical cleaning action, C_M is the cost of a mechanical cleaning action, C_E is the cost of thermal energy and j is the number of chemical cleaning actions. Subscripts C and M denote chemical and mechanical cleaning, respectively. The chemical cleaning actions are assumed to partially clean the exchangers leaving any coke formed at the time of the cleaning action. It is assumed that the mechanical cleaning action would bring the exchanger to the original clean state, resetting the super-cycle.

A generalized method of the use of Equation (15) was discussed in Ishiyama et al. [16], where dimensionless parameters were introduced to define exchanger operation and performance. They used a graphical solution to provide a rule of thumb for the number of chemical cleaning actions required before performing a mechanical cleaning action. For the exchanger in this case study, the dimensionless parameters required to identify the super-cycle time are summarized in Table 4. Using these parameters and the graphical approach in Ishiyama et al. [16], the super-cycle period was identified to be about 350 days, with no

chemical cleaning actions (in contrast to Figure 7, which shows a combination of chemical and mechanical cleaning).

Figure 8 compares the heat duty of the current and the proposed cleaning schedules using the historical plant data. The analysis gives ϕ_{super} of 600 US$ day^{-1} for the proposed schedule (an annual mechanical clean) compared to 710 US$ day^{-1} for the current cleaning schedule. The difference represents a net annual saving of about 40,000 US$, which would have to be considered along-side the impact of such a change in cleaning strategy on other operations in the refinery.

DISCUSSION

In Case Study 1, a range of deposit thermal conductivities were extracted from deposits formed on exchangers located downstream of the desalter. The values matched those reported in literature. Deposits exposed to higher surface temperatures showed a tendency to have a higher maximum thermal conductivity. Simulation of exchanger E45 with a range of λ_f is used to illustrate the importance of λ_f in thermo-hydraulic analysis: Figure 8 is a plot of Bi_f (defined in Equation (5)) against the ratio of the fouled and clean pressure drops ($\Delta P_{fouled}/\Delta P_{cl}$). It can be seen that λ_f determines whether the primary impact of fouling on exchanger performance is hydraulic or thermal. Figure 8 shows that low values of λ_f will result in the thermal limitation being met before the hydraulic limitation and vice versa.

The roughness of the surface was assumed to be constant during the analysis. The two roughness values, of 43 μm and 200 μm, were believed to cover the range of surface roughness that may be expected for the fouling layers. Dynamic variation in surface

roughness has been discussed elsewhere (e.g. [4]). However, the use of a constant value was deemed appropriate here as additional, unknown parameters would have to be introduced and these could not be independently verified.

Case Study 2 presented industrial exchanger data showing that aging of deposits does have a noticeable impact on the cleaning of such units. The difference between the mixed and mechanical-only cleaning cycles is not insignificant, and refineries should endeavor to use systematic methodologies to identify when to use which cleaning method. The case study considered only cleaning of a single exchanger: network interactions would need to be included to evaluate overall benefit to the preheat train, e.g. [17], [18].

CONCLUSIONS

Pressure drop data were used to estimate fouling deposit thicknesses in industrial heat exchangers. The calculated deposit thermal conductivity values lay between 0.1 and 0.9 $W\ m^{-1}\ K^{-1}$. The data sets also enabled the thermal conductivity of fresh deposits and some parameters of the aging model to be determined. Deposits exposed to higher surface temperatures showed a higher maximum thermal conductivity.

One case study confirmed that a deposit became harder to remove (to be cleaned) when exposed to a hotter surface for a prolonged period, reducing the effectiveness of a chemical cleaning step (gas oil wash). The information on deposit hardening (based on cleaning effectiveness) was used to identify the optimal type of cleaning method to use and the timing of cleaning events.

This manuscript illustrates the value of making pressure drop measurements on an operating plant, as the two-layer aging model could be parameterised without the thickness and thermal conductivity information.

ACKNOWLEDGMENTS

The authors wish to thank Preem Raffinaderi AB, Göteborg, Sweden, for supplying the monitoring data for the analysis.

NOMENCLATURE

A heat transfer area, m^2

a dimensional constant, kg m^{-3} s^{-2}

A_a prefactor of aging kinetic equation, $days^{-1}$

b dimensional constant, $m^{4.75 \sim 5}$ $s^{-(1.75 \sim 2)}$

Bi_f fouling Biot number

C_E energy cost, US$ J^{-1}

C_f friction factor, -

C_M, C_c cleaning cost, mechanical, chemical, US$ per clean

C_{min} minimum heat capacity flow, J K^{-1} S^{-1}

d tube diameter, m

E_a, E_F activation energy for aging, fouling, J mol^{-1}

h film transfer coefficient, W m^{-2} K^{-1}

j number of chemical cleaning actions

k_a aging decay constant, day^{-1}

k_c coking rate, m^2 K W^{-1} s^{-1}

k_g deposition rate, m^2 K W^{-1} s^{-1}

m mass flow rate, kg s^{-1}

Q heat duty, W

R gas constant, J mol^{-1} K^{-1}

R_f fouling resistance, m^2 K W^{-1}

$\dot{R}_f$ rate of change in overall fouling resistance, m^2 K J^{-1}

Re Reynolds number, -

t time, days

t_c, t_m operating time until clean (chemical, mechanical), days

t_{super} super-cycle duration, days

T temperature, K

U overall heat transfer coefficient, W m^{-2} K^{-1}

y youth factor, dimensionless

Greek Symbols

α deposition rate constant, m^2 K W^{-1} s^{-1}

δ deposit thickness, m

ε surface roughness, μm

ϕ_{super} super-cycle cost, US$ day^{-1}

ΔP pressure drop, Pa

ΔT_{max} maximum temperature difference, K

λ thermal conductivity, W m^{-1} K^{-1}

λ_f average deposit thermal conductivity, W m^{-1} K^{-1}

τ wall shear stress, Pa

τ_C, τ_M cleaning action duration (chemical, mechanical), days

Subscripts

c coke (final aged layer)

cl clean

eff effective value

i inner

f foulant layer

fouled fouled condition

film film layer

g gel (fresh layer)

o outer

super super-cycle

w wall

REFERENCES

[1] N. Epstein, "Thinking about heat transfer fouling: A 5 multiplied by 5 matrix," *Heat Transf. Eng.*, vol. 4, no. 1, pp. 43–56, Jan.-Mar. 1983. DOI: 10.1080/01457638108939594.

[2] E. M. Ishiyama, F. Coletti, S. Macchietto, W. R. Paterson, and D. I. Wilson, "Impact of deposit ageing on thermal fouling: Lumped parameter model," *AIChE J.*, vol. 56, no. 2, pp. 531–545, Feb. 2010. DOI: 10.1002/aic.11978.

[3] D. I. Wilson, E. M. Ishiyama, W. R. Paterson, and A. P. Watkinson, “Ageing: Looking back and looking forward,” presented at the International Conference on Heat Exchanger Fouling adn Cleaning VIII, Schaldming, Austria, June 2009.

[4] F. Coletti, E. M. Ishiyama, W. R. Paterson, D. I. Wilson, and S. Macchietto, “Impact of deposit aging and surface roughness on thermal fouling: Distributed model,” *AIChE J.*, vol. 56, no. 12, pp. 3257–3273, Dec. 2010. DOI: 10.1002/aic.12221.

[5] E. M. Ishiyama, W. R. Paterson, and D. I. Wilson, “Exploration of alternative models for the aging of fouling deposits,” *AIChE J.*, vol. 57, no. 11, pp. 3199–3209, Nov. 2011. DOI: 10.1002/aic.12514.

[6] G. T. Atkins, “What to do about high coking rates,” *PetroChem Eng.*, vol. 34, no. 4, pp. 20–25, Apr.1962.

[7] E. M. Ishiyama, W. R. Paterson, and D. Ian Wilson, “Optimum cleaning cycles for heat transfer equipment undergoing fouling and ageing,” *Chem. Eng. Sci.*, vol. 66, no. 4, pp. 604–612, Feb. 2011. DOI: 10.1016/j.ces.2010.10.036.

[8] T. Pogiatzis, E. M. Ishiyama, W. R. Paterson, V. S. Vassiliadis, and D. I. Wilson, “Identifying optimal cleaning cycles for heat exchangers subject to fouling and ageing,” *Appl. Energy*, vol. 89, no. 1, pp. 60–66, Jan. 2012. DOI: 10.1016/j.ces.2010.10.036.

[9] A. P. Watkinson, “Critical review of organic fluid fouling,” Argonne National Laboratory, Argonne, Final report, AWL/CNSV-TM-208, 1988.

[10] J. Sousa, M. da Conceicao Cunha, and A. Sa Marques, “An explicit solution to the Colebrook-White equation through simulated annealing,” in Water Industry Systems: modelling and optimization applications, D. A. Savic and G. A. Walters, Eds., Research Studies Press Ltd., UK, 1999, pp. 347–355.

[11] V. Gnielinski, “New equations for heat and mass transfer in turbulent pipe and channel flow,” *Int. Chem. Eng.*, vol. 16, pp. 359–368, 1976.

[12] ESDU, “Baffled shell-and-tube heat exchangers: flow distribution, pressure drop and heat transfer coefficient on the shellside,”, IHS, London, UK, Report 83038, 1984.

[13] R. K. Sinnott, *Coulson and Richardson’s Chemical Engineering: Chemical Engineering Design*, vol. 6, 2nd revised ed. Oxford, UK, Butterworth-Heinemann Ltd, 1996.

[14] E. M. Ishiyama, W. R. Paterson, and D. I. Wilson, “Thermo-hydraulic channelling in parallel heat exchangers subject to fouling,” *Chem. Eng. Sci.*, vol. 63, no. 13, pp. 3400–3410, Jul. 2008. DOI: 2010-01-16 12:20:13.

[15] E. M. Ishiyama, S. J. Pugh, W. R. Paterson, G. T. Polley, J. Kennedy, and D. I. Wilson, “Management of crude preheat trains subject to fouling,” *Heat Transf. Eng.*, vol. 34, no. 8–9, pp. 692–701, Feb. 2013. DOI: 10.1080/01457632.2012.739036.

[16] E. M. Ishiyama, W. R. Paterson, and D. I. Wilson, “Aging is important: Closing the fouling-cleaning loop,” *Heat Transf. Eng*., vol. 35, no. 3, pp. 311–326, Feb. 2014. DOI: 10.1080/01457632.2013.825192.

[17] A. L. Diaby, S. J. Miklavcic, and J. Addai-Mensah, “Optimization of scheduled cleaning of fouled heat exchanger network under ageing using genetic algorithm,” *Chem. Eng. Res. Des.*, vol. 113, pp. 223–240, Sep. 2016. DOI: 10.1002/apj.5500130103.

[18] L.-L. Liu, J. Fan, P.-P. Chen, J. Du, and F.-L. Yang, “Synthesis of heat exchanger networks considering fouling, aging, and cleaning,” *Ind. Eng. Chem. Res.*, vol. 54, no. 1, pp. 296–306, 2015. DOI: 10.1021/ie5027524.

1 Table 1: Reported thermal conductivity of fouling layer solids [9]

Material	Thermal conductivity (W $m^{-1}K^{-1}$)
Coke, carbon	1.7
Wax	0.23
Graphite	4.4
Pitch	0.1-0.2
Amorphous asphalt	0.17
Asphaltene	0.20
Oil	0.12
Hydrocarbon vapour	0.015
Deposit gas-oil fouling	0.46

2

3

4

5

1 Table 2: Heat exchanger average operating conditions

	Effective area per shell (m^2)	Clean overall heat transfer coefficient (W m^{-2} K^{-1})	Crude-side surface temperature (°C)	Crude-side surface shear stress (Pa)
E45	730	150 – 300	220 – 260	5 – 15
E5AB	405	80 – 200	180 – 240	0.1 – 5
E50ABC	260	100 – 500	160 – 235	0.1 – 4

2

3

1 Table 3 Summary of cleaning events marked in Figure 6.

Date	Cleaning event
17/03/2006 – 22/03/2006	A = Hydro blasting
22/07/2006 – 09/08/2006	B = Gas oil wash
25/03/2007 – 05/04/2007	C = Gas oil wash
08/01/2008 – 17/01/2008	D = Gas oil wash
28/10/2008 – 02/01/2009	E = Hydro blasting

2

3

Table 4: Parameters extracted for Case Study 2 to illustrate the optimal cleaning cycle.

Parameter	Value
$U_{cl}\,A\,/\,C_{\min}$	0.87
$Q_{cl}\,/(C_{\min}\,\Delta T_{\max})$	0.54
$\dot{R}_f U_{cl}\ \tau_M$	0.075
$C_M\,/\,(\tau_M\,Q_{cl}\,C_M)$	0.92
$\lambda_g\,/\,\lambda_c$	0.11
$C_C\,/\,C_M$	0.25
$k_g\,/\,k_c$	12
$\tau_C\,/\ \tau_M$	0.5

$C_{\min}$ = minimum heat capacity flow, A = heat transfer area, $\Delta T_{\max}$ = maximum temperature driving force; $\dot{R}_f$ = the total rate of change in fouling resistance.

List of Figures

Figure 1 Schematic layout of a section of the preheat train. The circles indicate shell-and-tube heat exchangers.

Figure 2 Effect of operating surface temperature on the estimated deposit thermal conductivity obtained from monitoring data from units E50ABC, E5AB and E45.

Figure 3 Extracted (i) fouling resistance, (ii) deposit thickness and (iii) deposit thermal conductivity for unit E45 over time period A. Filled circles show values calculated using a surface roughness of 43 μm; hollow circles show the results for a surface roughness of 200 μm. The error bars in (ii) and (iii) indicate the uncertainty in the calculation assuming an uncertainty in the measured pressure drop of ± 10 %.

Figure 4 Operating conditions in E45, time period A. (i) Surface temperature and (ii) Wall shear stress. Data presented for two surface roughness values (filled circle, 43 μm and hollow circle, 200 μm). The error bars in (ii) represent the uncertainty assuming an uncertainty in the measured pressure drop of ± 10 %.

Figure 5 E45 (i) Fouling resistance, (ii) deposit thickness and (iii) deposit thermal conductivity in time period B. Filled circle – calculated using a surface roughness of 43 μm; hollow circle - 200 μm). The error bars associated with (ii) and (iii) represent the uncertainty in the calculation assuming an uncertainty in the measured pressure drop of ± 10 %. Dashed and continuous lines represent the predictions of the distributed model (Equation (13)).

Figure 6 Overall heat transfer coefficient and fouling resistance for case study exchanger. Labels A, B, C, D and E indicate cleaning actions (see Table 3). Filled squares and hollow circle denote mechanical and chemical cleaning events, respectively. The dashed line indicates the trend in the fouling resistance immediately after cleaning.

Figure 7 Heat duty variation over time. Hollow circles show data for current cleaning schedule (three gas oil washes between hydro-blasting). The dashed line represents the performance for the proposed cleaning schedule.

Figure 8 Thermal performance (Bi_f) against hydraulic performance ($\Delta P_{fouled}/\Delta P_{cl}$) of exchanger E4 for different deposit thermal conductivities.

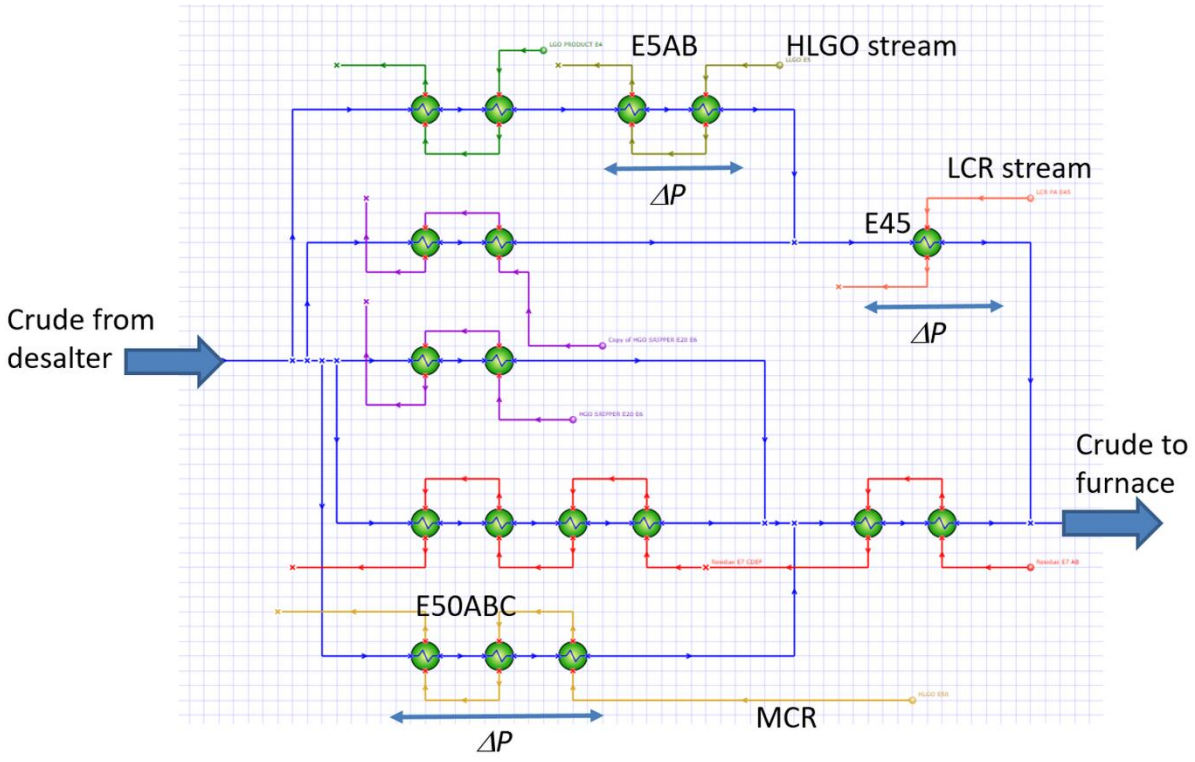

Figure 1 Schematic layout of a section of the preheat train. The circles indicate shell-and-tube heat exchangers.

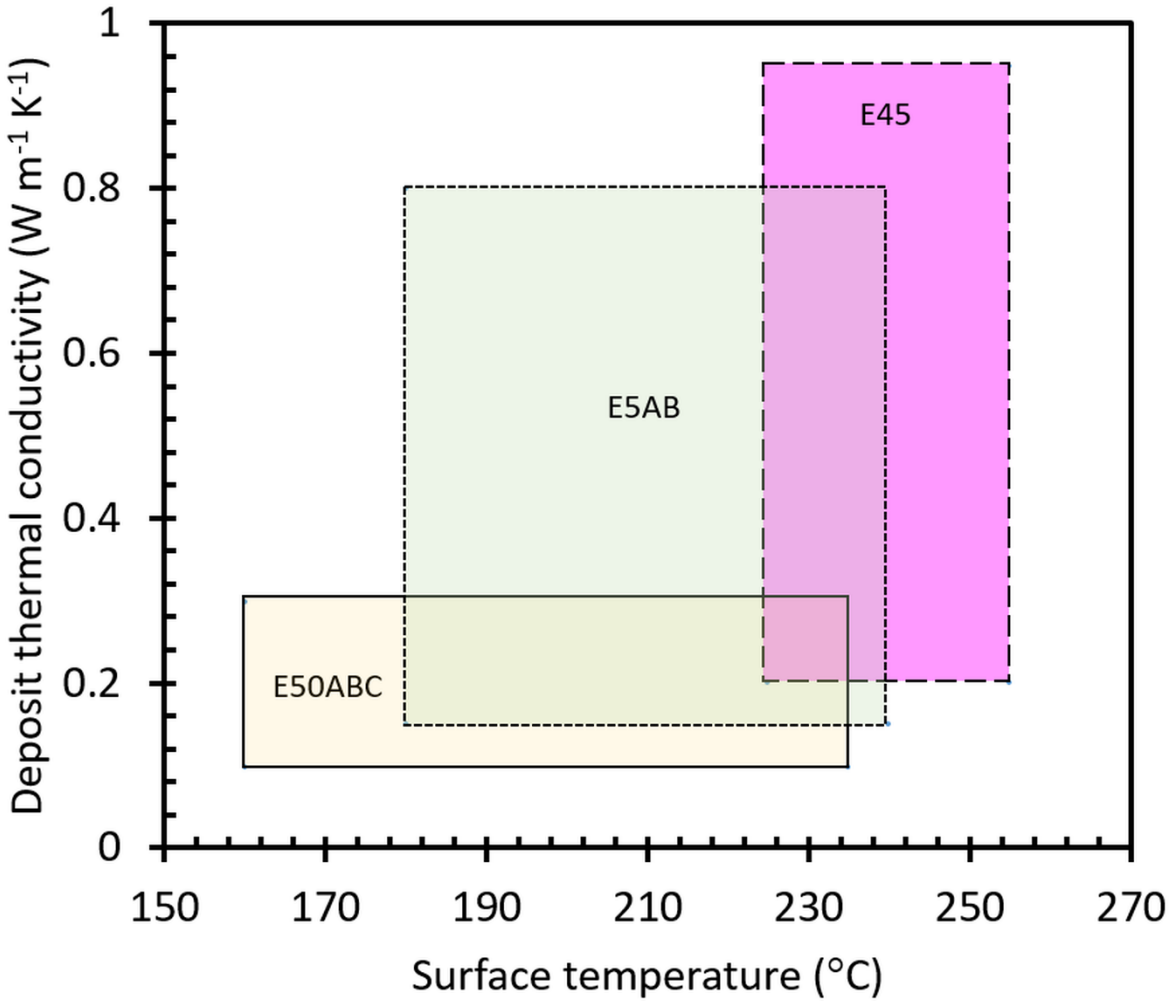

Figure 2 Effect of operating surface temperature on the estimated deposit thermal conductivity obtained from monitoring data from units E50ABC, E5AB and E45.

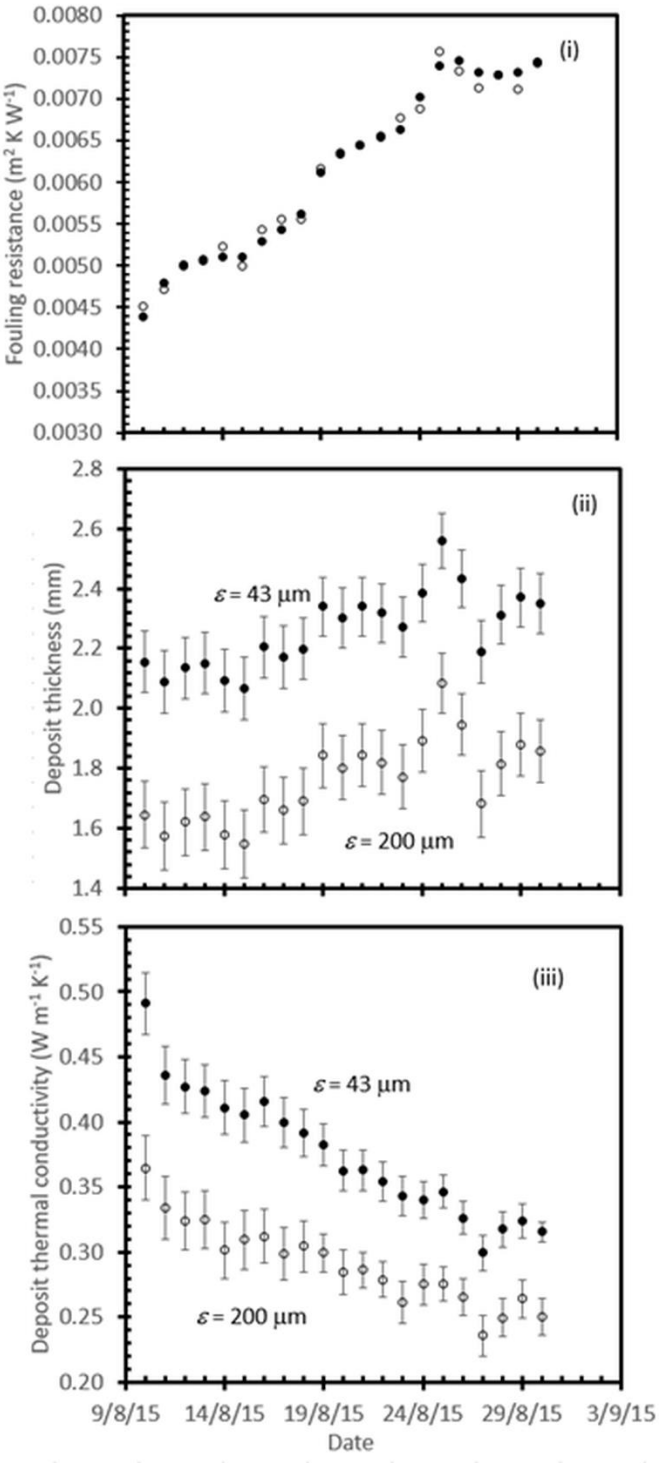

Figure 3 Extracted (i) fouling resistance, (ii) deposit thickness and (iii) deposit thermal conductivity for unit E45 over time period A (sharing a common date axis). Filled circles show values calculated using a surface roughness of 43 µm; hollow circles show the results for a surface roughness of 200 µm. The error bars in (ii) and (iii) indicate the uncertainty in the calculation assuming an uncertainty in the measured pressure drop of ± 10 %.

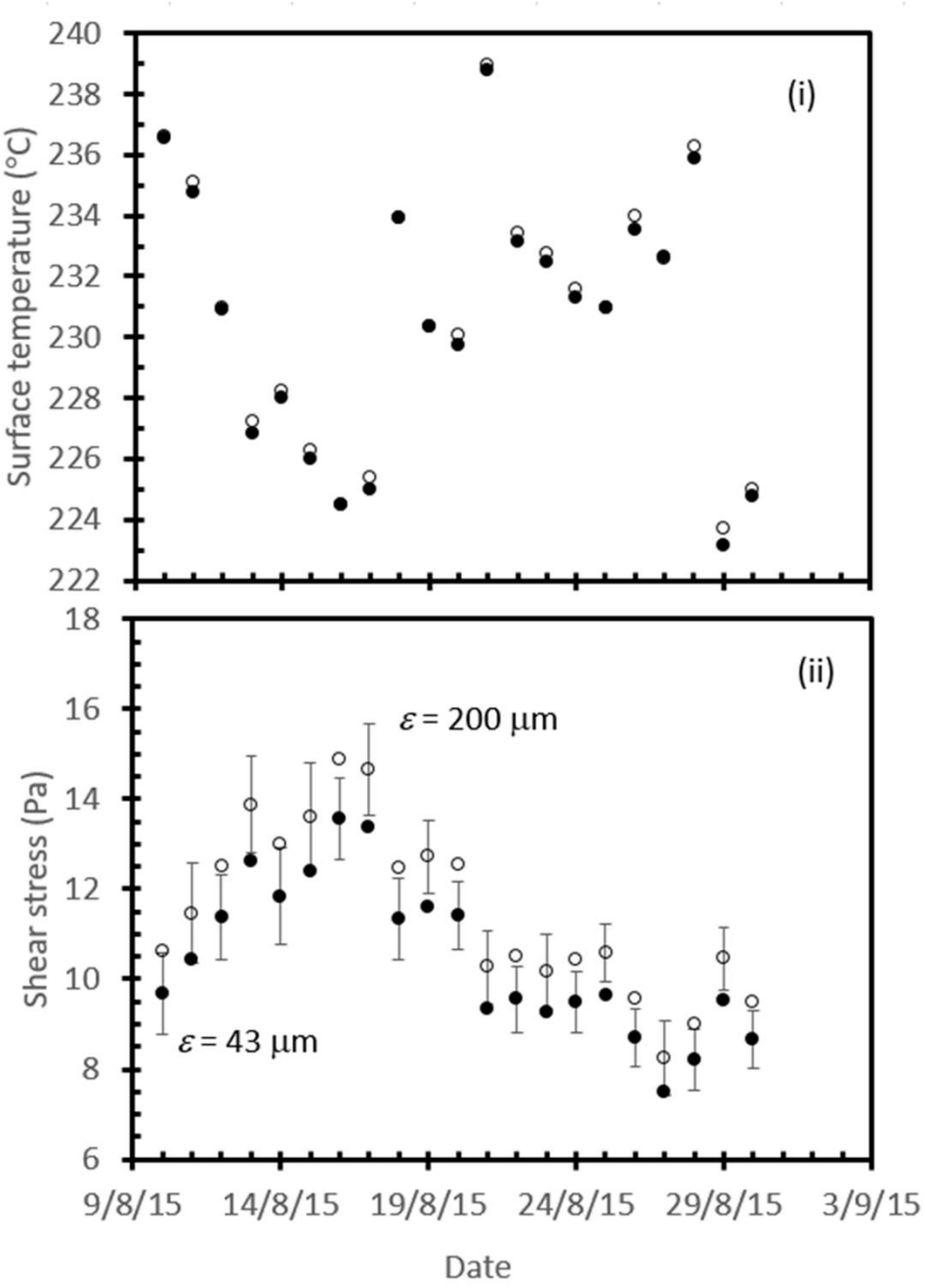

Figure 4 Operating conditions in E45, time period A. (i) Surface temperature and (ii) Wall shear stress. Data presented for two surface roughness values (filled circle, 43 μm and hollow circle, 200 μm). The error bars in (ii) represent the uncertainty assuming an uncertainty in the measured pressure drop of ± 10 %.

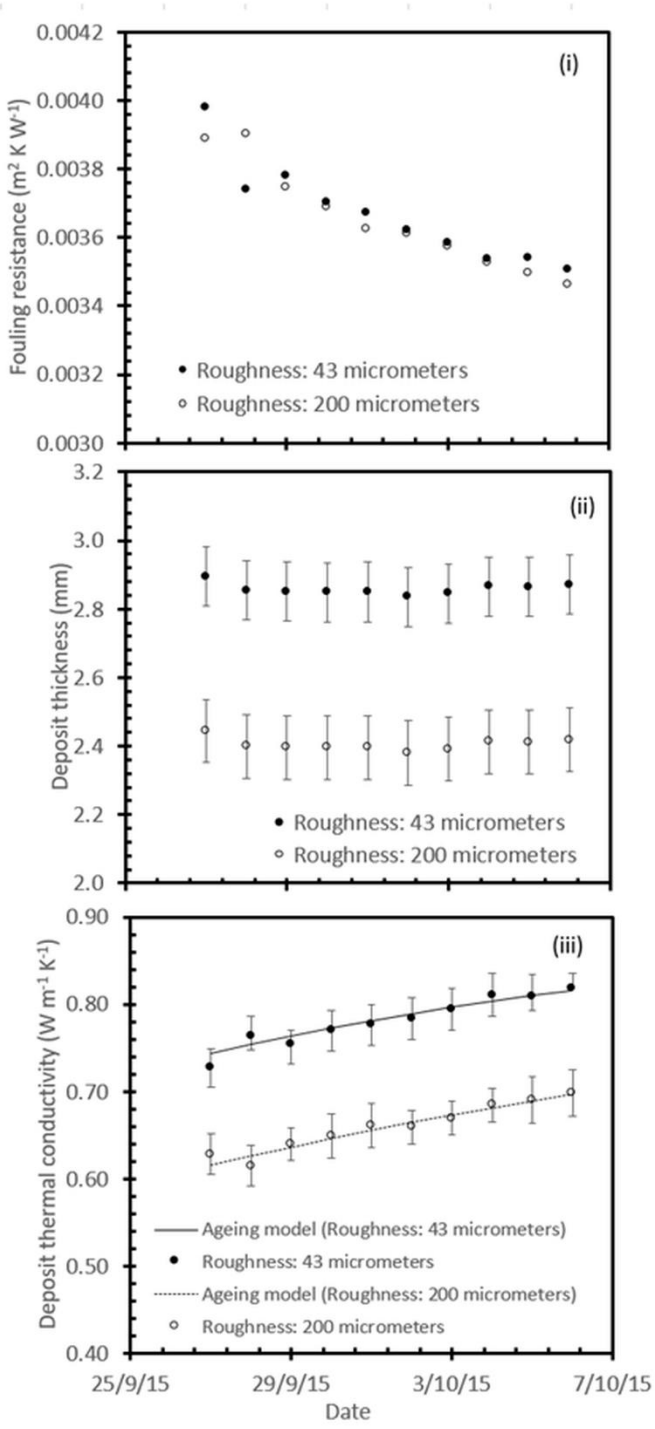

Figure 5 E45 (i) Fouling resistance, (ii) deposit thickness and (iii) deposit thermal conductivity in time period B. Filled circle – calculated using a surface roughness of 43 μm; hollow circle - 200 μm). The error bars associated with (ii) and (iii) represent the uncertainty in the calculation assuming an uncertainty in the measured pressure drop of ± 10 %. Dashed and continuous lines represent the predictions of the distributed model (Equation (13)).

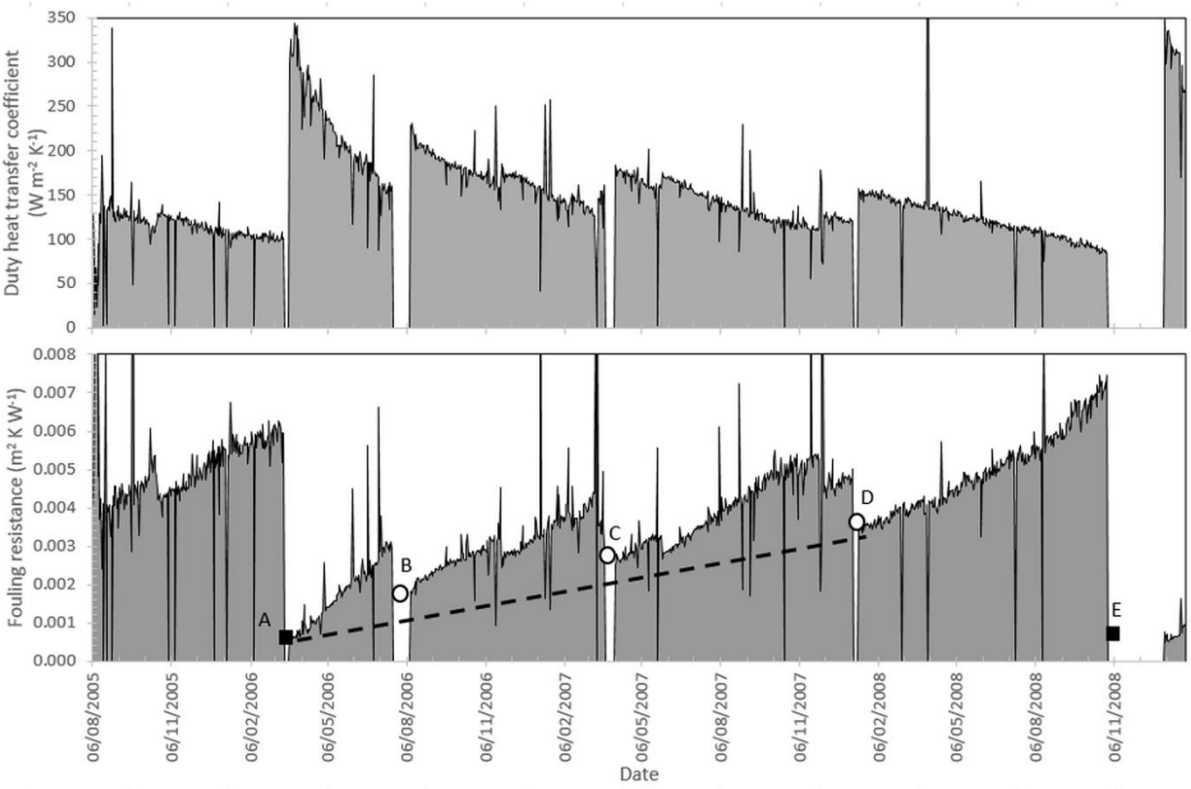

Figure 6 Overall heat transfer coefficient and fouling resistance for case study exchanger. Labels A, B, C, D and E indicate cleaning actions (see Table 3). Filled squares and hollow circle denote mechanical and chemical cleaning events, respectively. The dashed line indicates the trend in the fouling resistance immediately after cleaning.

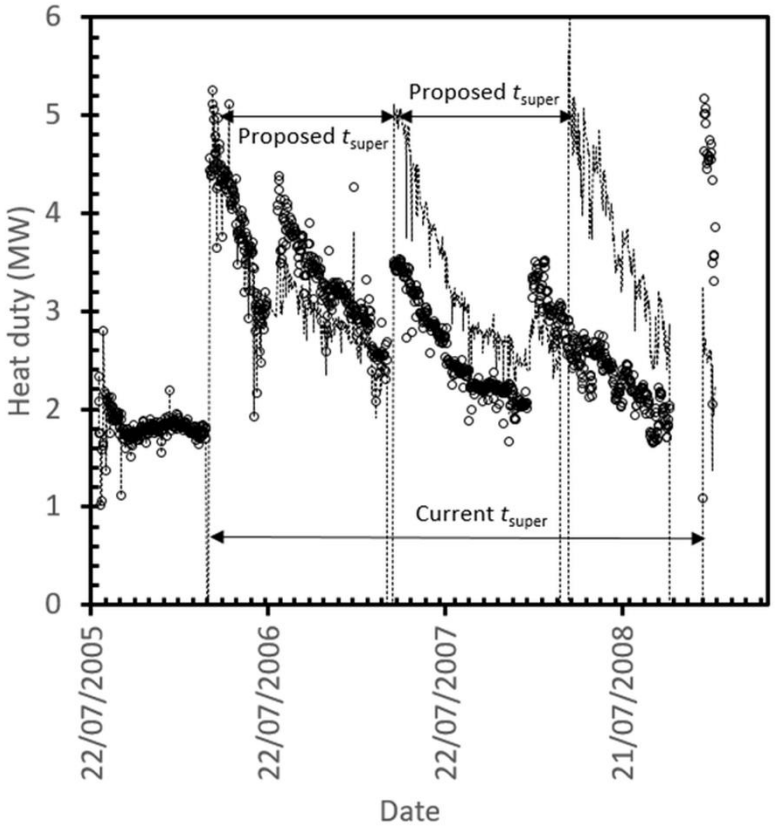

Figure 7 Heat duty variation over time. Hollow circles show data for current cleaning schedule (three gas oil washes between hydro-blasting). The dashed line represents the performance for the proposed cleaning schedule.

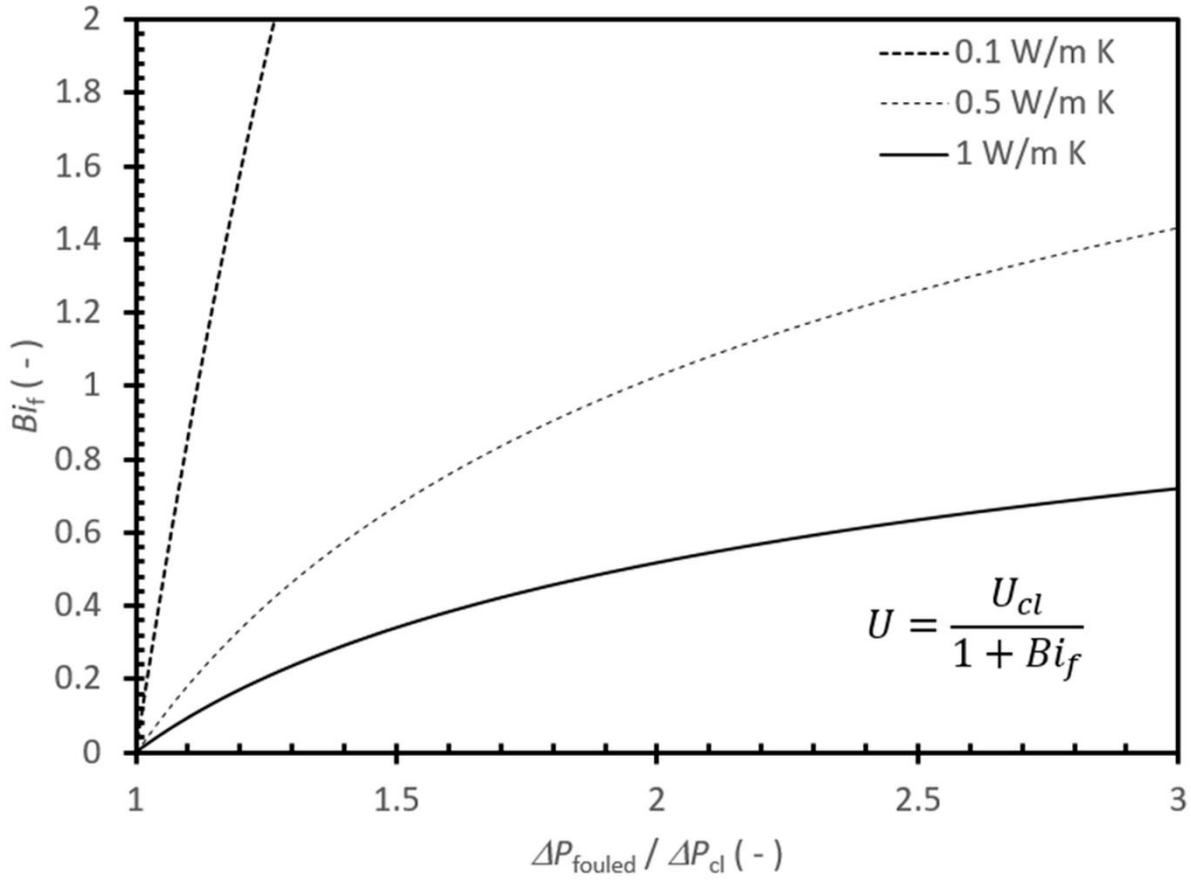

Figure 8 Thermal performance (Bi_f) against hydraulic performance ($\Delta P_{fouled}/\Delta P_{cl}$) of exchanger E4 for different deposit thermal conductivities.

Edward Ishiyama is a Senior Research Project Engineer at HTRI. He holds a PhD in Chemical Engineering from the University of Cambridge, United Kingdom. He has over 12 years of experience in applying heat transfer, process control, and thermodynamic principles to identify and solve problems associated with heat exchangers and heat exchanger networks subject to fouling.

7

Erik Falkeman is a senior process engineer at Preem AB, Göteborg, Sweden. He received his M.Sc. degree in Chemical Engineering with Engineering Physics in 2004 from Chalmers University of Technology, Göteborg, Sweden. He is currently responsible for the Crude Distillation Units (CDU) and the Distillate Hydrotreaters (DHT) at Preem refinery in Göteborg.

14

Ian Wilson is based in the Department of Chemical Engineering and Biotechnology at Cambridge. He joined the faculty in 1994 after completing his PhD at the University of British Columbia and holds a personal chair as Professor of Soft Solids and Surfaces. His research interests include fouling, cleaning, heat transfer, rheology and food engineering. Ian was awarded an ScD by Cambridge in 2013 for his work on fouling and cleaning.

15

Simon Pugh is Senior Product Lead for SmartPM at HTRI and holds a Mechanical Engineering degree from Brunel University,

United Kingdom. With over 35 years' experience collaborating with engineers from industry, he has led the development and application through consulting of new methods and software for better heat exchanger selection, design, and operation. His work on crude oil fouling led to the development of the SmartPM software for improved refinery preheat train management. Before joining HTRI in 2016, he was Director of Process Engineering in IHS Downstream Research.